Low-Temperature High-Mobility Amorphous IZO for Silicon Heterojunction Solar Cells

Monica Morales-Masis, Silvia Martin de Nicolas, Jakub Holovsky, Stefaan De Wolf, and Christophe Ballif

Abstract— Parasitic absorption in the transparent conductive oxide (TCO) front electrode is one of the limitations of silicon heterojunction (SHJ) solar cells efficiency. To avoid such absorption while retaining high conductivity, TCOs with high electron mobility are preferred over those with high carrier density. Here we demonstrate improved SHJ solar cell efficiencies by applying high mobility amorphous indium zinc oxide (a-IZO) as the front TCO. We sputtered a-IZO at low substrate temperature and low power density, and investigated the optical and electrical properties as well as sub-band tail formation - quantified by the Urbach energy (E_U) – as a function of the sputtering oxygen partial pressure. We obtain a E_U as low as 128 meV for films with the highest Hall mobility of 60 cm²/Vs. When comparing the performance of a-IZO films with ITO and IO:H, we find that IO:H (115 cm²/Vs) exhibits a similar E_U of 130 meV, while ITO (25 cm 2 /Vs) presents a much larger E_U of up to 270 meV. The high film quality, indicated by the low E_U , the high mobility and low free carrier absorption of the developed a-IZO electrodes result in a significant current improvement, achieving conversion efficiencies over 21.5%, outperforming those with standard ITO.

Index Terms—amorphous indium zinc oxide, electron mobility, heterojunction, indium tin oxide, silicon, solar cells, transparent conductive oxides, Urbach energy.

I. INTRODUCTION

Transparent conductive oxides (TCOs) used as front electrodes in solar cells should simultaneously feature high lateral electrical conductivity, low contact resistance with the adjacent layers, low optical absorption from the UV to the IR, and an appropriate refractive index for maximal

Date of submission:

This work was financially supported by Axpo Naturstrom Fonds; CCEM CONNECT PV; the European Commission (FP7 projects HERCULES, Grant 608498; CHEETAH Grant 609788) by the Office Fédéral de l'énergie (OFEN); by the DOE FPaceII project; by the Czech Science Foundation grant no GA14-05053S; and by the Swiss National Science Foundation (SNSF) for partial support on equipment acquisition.

M. Morales-Masis, S. Martin de Nicolas, S. De Wolf and C. Ballif are with the Photovoltaics and Thin-Film Electronics Laboratory (PVLab), Institute of Microengineering (IMT), Ecole Polytechnique Fédérale de Lausanne (EPFL), CH-2002 Neuchatel, Switzerland (email: monica.moralesmasis@epfl.ch, silvia.martin-de-nicolas@epfl.ch, stefaan.dewolf@epfl.ch, christophe.ballif@epfl.ch).

J. Holovsky is with the Institute of Physics ASCR, v. v. i., Cukrovarnická 10, 162 00 Prague, Czech Republic and the Czech Technical University in Prague, Faculty of Electrical Engineering, Technická 2, 16627 Prague, Czech Republic (email: holovsky@fzu.cz).

light in-coupling. However, these properties may conflict with each other. For example, improving the conductivity by increasing the free carrier density inevitably leads to higher absorption in the IR. This explains the search for TCOs with high electron mobility [1-4]. Additionally, due to the presence of temperature sensitive layers in many solar cell designs (for example in thin-film silicon (Si) [5], Si heterojunction [6], CIGS [7], polymer [8] and perovskite solar cells [9]), low temperature deposition methods are needed, which might result in TCOs with amorphous structure. The intrinsic disorder of amorphous materials may, however, restrict the carrier mobility.

Several deposition techniques have been explored to fabricate high mobility TCOs at low temperatures, including, sputter deposition [10-12], chemical vapor deposition (CVD) [13], solution process [14] and atomic layer deposition (ALD) [15,16]. Among this variety of methods, sputtering is the most established deposition technique, despite the fact it can lead to damage of underlying layers [17]. 'Soft' sputtering can further mitigate this potential issue.

In this article, we study the properties of amorphous indium zinc oxide (a-IZO) thin films grown by RF sputtering as a high-mobility amorphous TCO. Using different oxygen partial pressures, we sputtered a-IZO films with a range of optoelectronic properties, and we study the correlations between its carrier mobility and Urbach energy, E_U . The latter parameter quantifies the combined broadening of conduction and valence band tails and scales directly with the degree of disorder or defects in a material [18-21].

To validate the use of a-IZO as front electrode, we also compared the performance of our a-IZO films with indium tin oxide (ITO) and hydrogenated indium oxide (IO:H), typically used as front electrodes in high efficiency c-Si heterojunction (SHJ) solar cells [6,22]. We found that the a-IZO films feature Urbach tails as low as the high-mobility (polycrystalline) IO:H. Furthermore, when applied as front electrodes in SHJ solar cells, the a-IZO front electrodes showed low contact resistance at the interface with the metal grids, representing an advantage over IO:H [22]. An improvement in the shortcircuit current densities (J_{sc}) is also observed in comparison with the cells with polycrystalline ITO. In addition, whereas the ITO films require an annealing step of 200 °C to improve their optoelectronic properties, the a-IZO films present excellent properties already in the as-deposited state. This makes a-IZO attractive for a large range of temperature sensitive applications. Finally, we show that sputtered a-IZO

thin films, due to the high mobility, fulfill the requirements as a front electrode in SHJ solar cells enabling conversion efficiencies above 21.5%.

II. EXPERIMENTAL DETAILS

The *a*-IZO films were fabricated by RF sputtering of an IZO target (90 wt% In_2O_3 and 10 wt% ZnO) at a substrate temperature of 60 °C. The RF power density was 1.9 W/cm² and the oxygen to total flow ratio, $r(O_2) = O_2/(Ar+O_2)$, introduced during the deposition was varied from 0.1% to 0.6%. All films were 100 ± 5 nm thick.

The ITO and IO:H samples were fabricated by DC and RF sputtering respectively under optimized oxygen conditions at room temperature. Details of the deposition parameters can be found in reference [22].

For the electrical and optical characterization of the films, the TCOs were deposited onto glass substrates, and for the photothermal deflection spectroscopy (PDS) measurements onto fused silica substrates. The TCOs were characterized before and after annealing (in air at 190 °C for 20 minutes), simulating the TCO properties after full SHJ solar cell fabrication [6].

The crystal structure of the films was analyzed by X-ray diffraction (XRD) using the grazing incidence (GI) mode. The electrical resistivity (ρ), carrier concentration (N_e) and Hall mobility (μ_{Hall}) were measured by Hall-effect in the van der Pauw configuration. The optical transmittance (T) and reflectance (R) of the films were measured by an UV-vis-NIR spectrometer with an integrating sphere, and the absorptance was determined from 100-T-R.

PDS was performed by an in-house developed system based on a 150W Xenon lamp. Fluorinert FC-72 was used as a temperature sensitive liquid. The principles of the PDS technique can be found in [23]. The transmittance and reflectance were measured simultaneously, and the absorption coefficient was evaluated as described in [24], corrected for second order terms, whereas the refractive index was simulated by a Drude model in a form taken from [25]. The thickness and refractive index parameters were varied to obtain the best fit to the measured transmittance and reflectance data.

SHJ solar cells were fabricated on high quality n-type float zone (FZ) c-Si wafers (<100>; 250µm; 1-5 Ω •cm). The wafers were randomly textured in an alkaline solution, wetchemically cleaned and dipped in hydrofluoric acid (HF) prior to plasma-enhanced chemical vapor deposition (PECVD) of intrinsic and doped hydrogenated amorphous silicon layers (a-Si:H). a-IZO or ITO films were used as the front electrode and deposited through a shadow mask (2×2 cm²), defining the device size. On the rear side of the wafer a TCO layer was used in all devices, followed by a silver back reflector also sputtered immediately after the back TCO. A silver front grid was screen-printed on the front of the 4 TCO pads, and the solar cells were cured for 20 minutes at 190 °C. Further details about the fabrication process can be found elsewhere [6]. Finally, the complete solar cells were characterized by current-

voltage (J-V) measurements on a sun simulator under Air Mass 1.5 global illumination.

III. RESULTS AND DISCUSSION

A. a-IZO: Structural, Electrical and Optical Properties

Figure 1 shows the GI-XRD patterns of the a-IZO films deposited with various $r(O_2)$. For all the samples, a broad peak centered at $2\theta = 32^{\circ}$ with an average full width at half maximum (FWHM) of 3.6° is observed. The large FWHM and the position of the peak indicate that the layers, as-deposited and annealed, are amorphous [11].

The electrical properties of the as-deposited and annealed a-IZO layers as a function of $r(O_2)$ are presented in Fig. 2a and b. As observed in Fig. 2a, the ρ does not change significantly except above $r(O_2) = 0.40\%$. This effect is given by the competing trends of N_e and μ_{Hall} (Fig. 2b). For the range of $r(O_2)$ studied, the N_e decreases with increasing $r(O_2)$, from 4.8 down to 0.2 x 10²⁰ cm⁻³ for the as-deposited films. The annealed films follow the same trend. The μ_{Hall} reaches a maximum of 60 cm²/Vs for r(O₂) of 0.4%, above and below which it slightly drops. We furthermore plotted the dependence of μ_{Hall} with N_e in Fig. 2c. We observed an initial increase in μ_{Hall} with increasing N_e up to 2 x 10^{20} cm⁻³. For N_e $> 2 \times 10^{20} \text{ cm}^{-3}$, μ_{Hall} decreases from 60 down to 40 cm²/Vs. The rise and subsequent decrease of μ_{Hall} with N_e , could be explained by the presence of different scattering mechanisms. At low N_e (< 2 x 10^{20} cm⁻³), possible μ_{Hall} limiting factors are potential barriers (percolation-type conduction) or latticescattering effects (phonon-like scattering) [26]. While for high N_e (> 2 x 10^{20} cm⁻³) ionized impurity scattering is the main limiting factor of μ_{Hall} [10,27,28]. Lennheer et al. has shown that for a-IZO the maximum μ_{Hall} is achieved when carrier transport is mainly limited by phonon-scattering, i.e. metallike transport and before ionized impurity scattering limits μ_{Hall} [28]. This maximum in μ_{Hall} is reached for a N_e of 1-2 x 10²⁰ cm⁻³, in accordance with our results. Fig. 2d displays the optical transmittance and absorptance of the a-IZO films with varying $r(O_2)$. All the films present a high transmittance (>75 %) in the visible and NIR region of the spectra. In the UV-Vis range we observe the well-known Burstein-Moss shift, i.e. a blue shift with increasing N_e (or decreasing $r(O_2)$) [29,30]. A clearer picture of the band-edge shift with increasing N_e is observed in the Tauc plot (Fig. 3a), discussed below. The optical absorptance of the films in the NIR strongly increases with decreasing $r(O_2)$. This is due to an increase in free carrier absorption associated with the increase in N_e . Note that the a-IZO $r(O_2) = 0.10\%$ already shows higher absorptance in the Vis range compared to the rest of the layers.

Based on the previous measurements, we selected three *a*-IZO films with $r(O_2) = 0.10$, 0.36 and 0.40% and measured by PDS. Results concerning their optical band gap (E_g) , absorption coefficient (a) and Urbach energy (E_U) are presented in Fig. 3.

We evaluated E_g following the Tauc relation, $a \propto (hv - E_g)^x$, with a the absorption coefficient and hv the photon energy.

The value of the exponent x changes according to the nature of absorption transitions: x=1/2 for allowed direct optical transitions, x=3/2 for forbidden direct optical transitions, and x=2 for indirect transitions [31]. For a-IZO, as well as several amorphous and crystalline TCOs, it has been demonstrated that electron momentum is largely conserved. Therefore, a direct band gap optical absorption model, with $a \propto (hv - E_g)^{1/2}$, closely describes the absorption edge of a-IZO [27,28,32,33].

The determined E_g values from the intercept of $a^2 = 0$ (Fig. 3a), for as-deposited as well as annealed films (the later indicated in parenthesis), are 3.6 eV (3.64 eV) for the sample with $r(O_2)$ of 0.10%, 3.49 eV (3.52 eV) for $r(O_2)$ of 0.36%, and 3.44 eV (3.48 eV) for $r(O_2)$ of 0.40%. The measured E_g is in close agreement with values reported in the literature [10]. The band gap blue-shift with increasing N_e is described by the Burstein-Moss shift as commented earlier. There is no significant shift between the as-deposited and annealed samples, confirming the results from the Hall effect measurements. The refractive index (n) of the films show a shift towards lower n values with increasing N_e consistent with the Drude model.

We furthermore extracted E_U following the Urbach relation, $a=Aexp(-hv/E_U)$, where A and E_U are constants and E_U represents the width of the tail states. The fitted slope used to obtain E_U is indicated by points in Fig. 4a. It is clear from the plot that the slope steepens, and therefore E_U decreases, with increasing oxygen content in the film. The obtained E_U values range from 225 meV for the film with $r(O_2)$ of 0.10% down to 128 meV for the film with $r(O_2)$ of 0.4%.

Sub-band tails (quantified by E_U) are characteristic of disorder in amorphous semiconductors. For the specific case of TCOs, it is proposed that these tails are mainly caused at the valence band (VB) tail, and those tails at the conduction band (CB) are much smaller. The low tailing at the conduction band is explained by the spherical 4s or 5s orbitals of the metal atoms forming the CB, which are less sensitive to disorder than the O 2p orbitals forming the VB [26]. This contribution from CB and VB tails, though, cannot be separated from our optical measurements. Importantly, several recent reports [21,34,35] proposed that under-coordinated oxygen, formation of metal pairs (e.g. In-In, In-Zn) or even sub-nanometer metal inclusions in amorphous TCOs will induce tail-like optical absorptions as well as deep defect levels close to the VB and CB edge [21,35,36]. The formation of sub-nanometer scale metal clusters inside the amorphous matrix, might affect the average atomic coordination, i.e. locally modify the structural properties of the films [37] influencing E_U . The formation of metal pairs or inclusions within the amorphous TCO matrix will also limit the carrier mobility due to electron scattering. This could explain why with increasing oxygen content, the formation of metal inclusions is reduced and the mobility of the films improves. Increasing the oxygen content will then allow the μ_{Hall} improvement, as observed in Fig. 2.b for $r(O_2) < 0.4$, and the decrease in E_U as commented above. While this correlation is clearly observed in Fig. 4b, further studies are required to evaluate this preliminary conclusion and a complete analysis

on this topic will be presented elsewhere.

B. Comparison with ITO and IO:H

In this section we compare the studied *a*-IZO thin films to ITO and IO:H, typically used as front electrodes in SHJ solar cells [6,22].

For this comparison, all the films have similar N_e after the annealing step, optimized to achieve low optical absorptance in the IR (Fig. 5), and the same thickness (100 \pm 5 nm on glass), optimized to reduce reflectance losses with a reflection minimum near 600 nm when used on our textured SHJ solar cells [38].

The sheet resistance (R_{sh}) of the layers is different for the three TCOs due to their different μ_{Hall} . The maximum μ_{Hall} after annealing is found for IO:H with 115 cm²/Vs, followed by a-IZO ($r(O_2) = 0.40\%$) with 60 cm²/Vs and finally ITO with the lowest μ_{Hall} of 25 cm²/Vs. The overview of the electrical properties of the ITO, IO:H and a-IZO films, before and after annealing, is presented in Table 1. Note that while ITO and IO:H are both polycrystalline after the annealing step, the IZO films remain amorphous (Fig. 6).

It is worth noting from Table 1 and Fig. 5 that *a*-IZO presents excellent optoelectronic properties already from the as-deposited step, presenting an advantage over IO:H and ITO. Considering also that the deposition is performed at substrate temperatures below 60 °C and at low power densities, *a*-IZO presents ideal properties for application in several temperature and damage sensitive technologies, like polymer and perovskite solar cells, flexible and paper electronics among others.

We furthermore performed PDS measurements of the ITO and IO:H samples, before and after annealing. The summary of the extracted E_g and E_U for each of the films and their comparison with the a-IZO films are presented in Fig. 7a and 7b respectively.

Starting with E_g , we observed a shift to larger gaps for both ITO and IO:H after annealing. While for ITO the shift of E_g to higher energies can be attributed to the Burstein Moss shift due to the increase in N_e with annealing (Table 1), in IO:H the shift of E_g to higher energies cannot be attributed to the same effect. Instead this shift may be caused by the amorphous to crystalline phase transition induced by the annealing step at 190 °C [12,39]. This phase change is clearly seen in the XRD data presented in Fig. 7. Note that for a-IZO and ITO no phase change is observed. Finally, the a-IZO films only present a small shift in E_g after annealing.

Following with the Urbach tail, we found the largest E_U for ITO in the as-deposited state, with only a small drop from 300 to 270 meV after annealing. As proposed previously by several groups, the incorporation of Sn into In_2O_3 leads to severely extended tail states in ITO [40], similar to the case of SnO_2 [41]. The extended tail states have been explained mainly as originating from ionized impurities, although other mechanisms like phonon scattering and excitonic effects have also been considered [40]. Remarkably, although the presence of the extended tail states has been widely commented in literature, to our knowledge, there are no reports of measured E_U values for sputtered ITO.

Contrary to ITO, we measured much lower E_U values for IO:H, which are very close to those measured for a-IZO with

 $r(O_2) = 0.40\%$. The lowest E_U achieved is 130 meV for IO:H and 128 meV for a-IZO. We note that IO:H does not present a strong shift in E_U before and after annealing regardless of the phase transition from the amorphous to the polycrystalline phase (Fig. 6), which may be surprising. The high mobility of IO:H and its crystallization after annealing suggest passivation of defects and/or decrease disorder in the films, and therefore a clear lowering of E_U was expected. More investigations would be required to explain these results. It is also important to note that we achieve similar E_U values for a-IZO and IO:H, although IO:H presents μ_{Hall} twice as large as that of the a-IZO at $r(O_2) = 0.40\%$. This together with the advantage that a-IZO presents excellent optoelectronic properties already from the as-deposited state, confirms the strong potential of a-IZO as a replacement for ITO and/or IO:H as a front electrode for solar cells.

C. Application of a-IZO as Front Contact for SHJ Solar Cells

To validate the potential of a-IZO as transparent electrode for solar cells, we fabricated SHJ solar cells and used the a-IZO films with $r(O_2) = 0.10$; 0.36; 0.40% as the front TCO contact. The solar cell configuration is shown in Fig. 8a. The short-circuit current density (J_{sc}) , open-circuit voltage (V_{oc}) , fill factor (FF) and efficiency results are shown in Fig. 8. A reference device with front ITO is also shown for comparison.

The J_{sc} of the a-IZO-based devices, increases with increasing r(O2). Indeed, as observed in Fig. 2d, the a-IZO layers with lower oxygen ratios feature higher free carrier absorption causing parasitic losses in the device. The observed Burstein-Moss effect does not compensate these J_{sc} losses in the final device. In spite of the enhanced optical properties of the a-IZO films with higher $r(O_2)$, the electrical properties behave in the opposite direction, causing electrical losses in the device. FF decreases for the film with the higher oxygen content, $r(O_2) = 0.40\%$, which is well correlated with the decreasing N_e trend presented in Fig. 2b. However, the FFvalues for the three cells are still high and suggest a good contact resistance between the a-Si and the metal grid. This is an advantage over IO:H-based devices as reported in [22]. In comparison with the ITO-based devices, the a-IZO devices present a clear advantage mainly on improved J_{sc} (Fig. 8b). In addition, the lower R_{sh} of a-IZO (35, 40 and 50 Ω /sq for the films with r(O2) = 0.1%, 0.36% and 0.4% respectively) as compared to that of ITO (100 Ω/sq), would allow a further increase of the pitch size of the front metal grid electrode and with it an even further improvement in J_{sc} is expected for the *a*-IZO devices [42,43].

Finally, the best J_{sc} -FF compromise is found with the device featuring an a-IZO film with $r(O_2) = 0.36\%$, achieving an energy conversion efficiency of 21.5 %.

Comparing the results of the a-IZO cells with the record IO:H-based SHJ device reported by L. Barraud $et\ al.$ [22], no marked difference is observed in the J_{sc} of both cells. This is expected due to the low optical absorptance of IO:H and a-IZO (Fig. 5). Both devices have the same configuration and were fabricated in the same laboratory. The reported IO:H cells have J_{sc} values of 38.9 mA/cm², while the maximum J_{sc} of the a-IZO cells reported in this work is of 38.6 mA/cm². The main advantage of the front a-IZO electrodes in

comparison with the IO:H-front electrodes is that the former can be deposited on a single step process, it doesn't require of a capping layer to achieve good contact resistance with the metal grid, and it presents higher stability under damp heat conditions [44].

These results clearly demonstrate that the *a*-IZO films developed within this work present excellent performance as a front TCO contact in high-efficiency SHJ solar cells.

IV. CONCLUSION

In summary, we have shown the influence on the carrier transport properties and sub-band tail formation of the oxygen partial pressure applied during sputtering deposition of a-IZO thin films. With increasing the oxygen partial pressure, the Hall mobility increases while E_U decreases. The highest mobility achieved for the a-IZO films is $60 \text{ cm}^2/\text{Vs}$, corresponding to an E_U of 128 meV. Comparing to ITO and high mobility IO:H, a-IZO presents a much lower E_U and Hall mobility than ITO, while it presents similar E_U than IO:H, although IO:H is polycrystalline and has a higher mobility compared to a-IZO. When applied as front contact in SHJ solar cells, a-IZO presents the advantage of good contact resistance with the front metal grids contrary to the IO:H, and an improved J_{sc} as compared to the cells with ITO. The low temperature deposition and excellent optoelectronic properties of a-IZO already from the as-deposited state makes this an excellent front electrode for SHJ solar cells and a wide range of temperature sensitive devices like flexible OLEDs and perovskite solar cells.

ACKNOWLEDGMENT

We thank F. Dauzou and N. Holm for technical support, N. Badel, C. Allebé, F. Debrot and CSEM-coworkers for their support in the silicon heterojunction cell processing, S. Nicolay and F. Haug for helpful discussions, and Adam Purkrt for PDS measurements.

REFERENCES AND FOOTNOTES

- [1] H. Fujiwara and M. Kondo, "Effects of carrier concentration on the dielectric function of ZnO:Ga and In₂O₃:Sn studied by spectroscopic ellipsometry: Analysis of free-carrier and band-edge absorption", *Phys. Rev. B*, vol. 71, pp. 075109-1- 075109-10, Feb. 2005.
- [2] S. Calnan and A. N. Tiwari, "High mobility transparent conducting oxides for thin film solar cells", *Thin Solid Films*, vol. 518, pp. 1839-1849, Jan. 2010.
- [3] Z. C. Holman M. Filipic, A. Descoeudres, S. De Wolf, F. Smole, M. Topic, and C. Ballif, "Infrared light management in high-efficiency silicon heterojunction and rear-passivated solar cells", *J. Appl. Phys.*, vol. 113, pp. 013107-1 -013107-13, Jan. 2013.
- [4] K. M. Yu, M. A. Mayer, D. T. Speaks, H. He, R. Zhao, L. Hsu, S. S. Mao, E. E. Haller, and W. Walukiewicz, "Ideal transparent conductors for full spectrum photovoltaics", *J. Appl. Phys.*, vol. 111, pp. 123505-1 -123505-5, Jun. 2012.

- [5] A. Shah, P. Torres, R. Tscharner, N. Wyrsch, and H. Keppner, "Photovoltaic technology: The case for thin-film solar cells", *Science*, vol. 285, pp. 692-698, July 1999.
- [6] S. De Wolf, A. Descoeudres, Z. C. Holman, and C. Ballif, "High-efficiency silicon heterojunction solar cells: a review", *Green*, vol. 2, pp. 7-24, Feb. 2012.
- [7] H. Hagendorfer, K. Lienau, S. Nishiwaki, C. M. Fella, L. Kranz, A. R. Uhl, D. Jaeger, L. Luo, C. Gretener, S. Buecheler, Y. E. Romanyuk, and A. N. Tiwari, "Highly transparent and conductive ZnO:Al thin films from a low temperature aqueous solution approach", *Adv. Mater.*, vol. 26, pp. 632-636, 2014.
- [8] G. Li, R. Zhu, and Y. Yang, "Polymer solar cells", *Nat. Photonics*, vol. 6, pp. 153-161, Feb. 2012.
- [9] J. Burschka, N. Pellet, S. J. Moon, R. Humphry-Baker, P. Gao, M. K. Nazeeruddin, and M. Gratzel, "Sequential deposition as a route to high-performance perovskitesensitized solar cells", *Nature*, vol. 499, pp. 316-319, Jul. 2013.
- [10] R. Martins, P. Almeida, P. Barquinha, L. Pereira, A. Pimentel, I. Ferreira, and E. Fortunato, "Electron transport and optical characteristics in amorphous indium zinc oxide films", *J. Non-Cryst. Solids*, vol. 352, pp. 1471-1474, Jun. 2006.
- [11] M. P. Taylor, D. W. Readey, M. van Hest, C. W. Teplin, J. L. Alleman, M. S. Dabney, L. M. Gedvilas, B. M. Keyes, B. To, J. D. Perkins, and D. S. Ginley, "The remarkable thermal stability of amorphous In-Zn-O transparent conductors", *Adv. Funct. Mater.*, vol. 18, pp. 3169-3178, Oct. 2008.
- [12] T. Koida, M. Kondo, K. Tsutsumi, A. Sakaguchi, M. Suzuki, and H. Fujiwara, "Hydrogen-doped In₂O₃ transparent conducting oxide films prepared by solid-phase crystallization method", *J. Appl. Phys.*, vol. 107, pp. 033514 (2010).
- [13] L. Ding, S. Nicolay, J. Steinhauser, U. Kroll, and C. Ballif, "Relaxing the Conductivity/Transparency Trade-Off in MOCVD ZnO Thin Films by Hydrogen Plasma", *Adv. Funct. Mater.*, vol. 23, pp. 5177–5182, May 2013.
- [14] R. M. Pasquarelli, D. S. Ginley and R. O'Hayrea, "Solution processing of transparent conductors: from flask to film", *Chem. Soc. Rev.*, vol. 40, pp. 5406–5441, Mar. 2011.
- [15] J. A. Libera, J. N. Hryn and J. W. Elam, "Indium Oxide Atomic Layer Deposition Facilitated by the Synergy
- between Oxygen and Water", *Chem. Mater*, pp. 2150-2158, Mar. 2011.
- [16] B. Macco, Y. Wu, D. Vanhemel and W. M. M. Kessels, "High mobility In₂O₃:H transparent conductive oxides prepared by atomic layer deposition and solid phase crystallization", *Phys. Status Solidi RRL*, pp. 987-990, Oct. 2014.
- [17] B. Demaurex, J. P. Seif, S. Smit, B. Macco, W. M. M. Kessels, J. Geissbuhler, S. De Wolf, and C. Ballif, "Atomic-Layer-Deposited Transparent Electrodes for Silicon Heterojunction Solar Cells", *IEEE J. Photovolt.*, vol. 4, pp. 1387-1396, Nov. 2014.
- [18] J. I. Pankove, "Absorption edge of impure gallium arsenide", *Phys. Rev.*, vol. 140, pp. A2059-A2065, Dec. 1965. [19] F. Urbach, "The long-wavelength edge of photographic sensitivity and of the electronic absorption of solids", *Phys. Rev.*, vol. 92, pp. 1324, Oct. 1953.

- [20] S. Schonau, F. Ruske, S. Neubert, and B. Rech, "Analysis of Urbach-like absorption tails in thermally treated ZnO:Al thin films", *Appl. Phys. Lett.*, vol. 103, pp. 192108-1-192108-4, Nov. 2013.
- [21] K. Nomura, T. Kamiya, H. Yanagi, E. Ikenaga, K. Yang, K. Kobayashi, M. Hirano, and H. Hosono, "Subgap states in transparent amorphous oxide semiconductor, In-Ga-Zn-O, observed by bulk sensitive x-ray photoelectron spectroscopy", *Appl. Phys. Lett.*, vol. 92, pp. 2202117-1 -2202117-3, May 2008.
- [22] L. Barraud, Z. C. Holman, N. Badel, P. Reiss, A. Descoeudres, C. Battaglia, S. De Wolf, and C. Ballif, "Hydrogen-doped indium oxide/indium tin oxide bilayers for high-efficiency silicon heterojunction solar cells", *Sol. Energy Mater. Sol. Cells*, vol. 115, pp. 151-156, Aug. 2013.
- [23] A. C. Boccara, D. Fournier, and J. Badoz, "Thermopetical spectroscopy: Detection by the "mirage effect", *Appl. Phys. Lett.*, vol. 36, pp. 130-132, Jan.1980.
- [24] D. Ritter and K. Weiser, "Suppression of interference fringes in absorption measurements on thin films", *Opt. Commun.*, vol 57, pp. 336-338, Apr. 1986.
- [25] K. Postava, H. Sueki, M. Aoyama, T. Yamaguchi, K. Murakami, and Y. Igasaki, "Doping effects on optical properties of epitaxial ZnO layers determined by spectroscopic ellipsometry", *Appl. Surf. Sci.*, vol. 175-176, pp. 543-548, May 2001.
- [26] H. Hosono, "Ionic amorphous oxide semiconductors: Material design, carrier transport, and device application", *J. Non-Cryst. Solids*, vol. 352, pp. 851–858, Apr. 2006.
- [27] T. Koida, H. Shibata, M. Kondo, K. Tsutsumi, A. Sakaguchi, M. Suzuki, and H. Fujiwara, "Correlation between oxygen stoichiometry, structure, and opto-electrical properties in amorphous In₂O₃:H films", *J. Appl. Phys.*, vol. 111, pp. 063721-1 -063721-7, Mar. 2012.
- [28] A. J. Leenheer, J. D. Perkins, M. F. A. M. van Hest, J. J. Berry, R. P. O'Hayre, and D. S. Ginley, "General mobility and carrier concentration relationship in transparent amorphous indium zinc oxide films", *Phys. Rev. B.*, vol. 7, pp. 115215-1 –
- [29] E. Burstein, "Anomalous optical absorption limit in InSb", *Phys. Rev.*, vol. 93, pp. 632-633, Dec. 1953.

115215-5, Mar. 2008.

- [30] T. S. Moss, "The interpretation of the properties of indium antimonide", *Proc. Phys. Soc. B.*, vol. 67, pp. 775-782, Jun. 1954.
- [31] J. I. Pankove, *Optical Processes in Semiconductors*, Dover, New York, 1971.
- [32] J. R. Bellingham, W. A. Phillips, and C. J. Adkins, "Electrical and optical-properties of amorphous indium oxide", *J. Phys. Condens. Matter.*, vol. 2, pp. 6207-6221, Apr. 1990.
- [33] A. Walsh, J. L. F. Da Silva, S.-H. Wei, C. Körber, A. Klein, L. F. J. Piper, A. DeMasi, K. E. Smith, G. Panaccione, P. Torelli, D. J. Payne, A. Bourlange, and R. G. Egdell, "Nature of the band gap of $\rm In_2O_3$ revealed by first-principles calculations and x-ray spectroscopy", Phys. Rev. Lett., vol. 100, pp. 167402-1 167402-4, Apr. 2008.
- [34] T. Kamiya, K. Nomura, M. Hirano, and H. Hosono, "Electronic structure of oxygen deficient amorphous oxide semiconductor a-InGa ZnO_{4-x} : Optical analyses and first-

principle calculations", *Phys. Stat. Sol.* (c), vol. 5, pp. 3098-3100, Jun. 2008.

[35] W. Korner, D. F. Urban, and C. Elsasser, "Origin of subgap states in amorphous In-Ga-Zn-O", *J. Appl. Phys.*, vol. 114, pp. 163704-1 -163704-6, Oct. 2013.

[36] W. Körner, D. F. Urban and C. Elsässer, "Generic origin of subgap states in transparent amorphous semiconductor oxides illustrated for the cases of In–Zn–O and In–Sn–O", *Phys. Status Solidi A*, pp. 1-6, Feb. 2015.

[37] R. Khanal, D. B. Buchholz, R. P. H. Chang, and J. E. Medvedeva, "Composition-dependent structural and transport properties of amorphous transparent conducting oxides", Phys. Rev. B, vol. 91, pp. 205203-1 – 205203-13, May 2015.

[38] Z. C. Holman A. Descoeudres, L. Barraud, F. Z. Fernandez, J. P. Seif, S. De Wolf, and C. Ballif, "Current losses at the front of silicon heterojunction solar cells", *IEEE J. Photovolt.*, vol. 2, pp. 7-15, Jan. 2012.

[39] H. F. Wardenga, M. V. Frischbier, M. Morales-Masis, A. Klein, "*In Situ* Hall Effect Monitoring of Vacuum Annealing of In₂O₃:H Thin Films," *Materials*, vol. 8, pp. 561-574, Feb. 2015

[40] I. Hamberg and C. G. Granqvist, "Evaporated Sn-doped In₂O₃ films - Basic optical properties and applications to energy-efficient windows", *J. Appl. Phys.*, vol. 60, pp. R123-R159, Aug. 1986.

[41] F. J. Arlingha, "Energy-bands in stannic oxide (SnO₂)", *J. Phys. Chem. Solids*, vol. 35, pp. 931-935, May 1974.

[42] J. Geissbühler, S. De Wolf, A. Faes, N. Badel, Q. Jeangros, A. Tomasi, L. Barraud, A. Descoeudres, M. Despeisse, and C. Ballif, "Silicon heterojunction solar cells with copper-plated grid electrodes: status and comparison with silver thick-film techniques", *IEEE J. Photovolt.*, vol. 4, pp. 1055-1062, Jul. 2014.

[43] M. Bivour, S. Schröer, M. Hermle, and S. W. Glunz, "Silicon heterojunction rear emitter solar cells: Less restrictions on the optoelectrical properties of front side TCOs", *Sol. Energy Mater. Sol. Cells*, vol. 122, pp. 120-129, Mar. 2014.

[44] T. Thosophon, S. De Wolf, M. Morales-Masis, and C. Ballif, "Stability of sputtered indium-oxide based electrodes", in preparation.



Monica Morales-Masis received her Ph.D. degree from Leiden University, Leiden, The Netherlands in January 2012, focusing on mixed conductor materials and resistive switching memories. In September 2012 she joined the Photovoltaics and Thin-Film Electronics Laboratory, Ecole Polytechnique Fédérale de Lausanne (EPFL), Neuchâtel,

Switzerland. Nowadays she is Team Leader for activities on transparent conductive oxides. Her current research interests include the fundamental investigation, design, fabrication and application of transparent conductive oxides for optoelectronic devices, including solar cells and light emitting diodes.



Silvia Martin de Nicolas Agut received the M.Sc. and Industrial Engineering degree in 2009 from Universitat Politècnica de Catalunya, Barcelona, Spain, focusing on renewable energies engineering. From 2009 to 2012 she was with the French National Institute for Solar Energy (CEA-INES), Le-Bourget-

du-Lac, France, where she carried out her Ph.D. on silicon heterojunction technology. In 2012 she received her Ph.D. degree in Physics from Université Paris XI, France. In 2013 she joined the Photovoltaics and Thin-Film Electronics Laboratory, École Polytechnique Fédérale de Lausanne, Neuchâtel, Switzerland, as a Postdoctoral Researcher, where she is working on high-efficiency silicon heterojunction devices.



Jakub Holovsky received the Ph.D. degree in 2012 from Charles University in Prague, Czech Republic, while he pursued the scientific work at Institute of Physics, Academy of Sciences of The Czech Republic v. v. i. and at Photovoltaics and Thin-Film Electronics Laboratory, Ecole Polytechnique Fédérale de Lausanne, Neuchâtel, Switzerland, where he also

spent one year as a SCIEX post-doc fellow. Since 2014 he teaches at Czech Technical University in Prague. He is focused on low absorption characterization methods for photovoltaic materials.



Stefaan De Wolf received his Ph.D. degree from the Catholic University of Leuven, Belgium, while he was with IMEC, developing crystalline silicon solar cells. From 2005 to 2008, he was with the National Institute of Advanced Industrial Science and Technology in Tsukuba, Japan, focusing on silicon heterojunction devices. In 2008, he joined

the Photovoltaics and Thin-Film Electronics Laboratory, École Polytechnique Fédérale de Lausanne, Neuchâtel, Switzerland, as a Team Leader for its activities on high-efficiency solar cells.



Christophe **Ballif** received the Graduate's degree in physics and Ph.D. from Ecole Polytechnique Fédérale de Lausanne (EPFL), Lausanne, Switzerland, in 1994 and 1998, respectively, focusing on novel photovoltaic materials. He was Postdoctoral Researcher at National Renewable Energy Laboratory, Golden,

CO, where he was involved in compound semiconductor solar cells (CIGS and CdTe). He then was with the Fraunhofer Institute for Solar Energy Systems, Freiburg, Germany, where he was involved in crystalline silicon photovoltaics (monocrystalline and multicrystalline) until 2003. He then joined the Swiss Federal Laboratories for Materials Testing

and Research, Thun, Switzerland, before becoming a Full Professor and Chair at the Institute of Microengineering, University of Neuchâtel, Neuchâtel, Switzerland, in 2004. In 2009, the Institute was transferred to EPFL. He is the Director of the Photovoltaics and Thin-Film Electronics Laboratory within the Institute as well as of the CSEM PV-center. His

research interests include thin-film solar cells, high-efficiency heterojunction crystalline cells, and module technology, contributing to technology transfer and industrialization of novel devices.

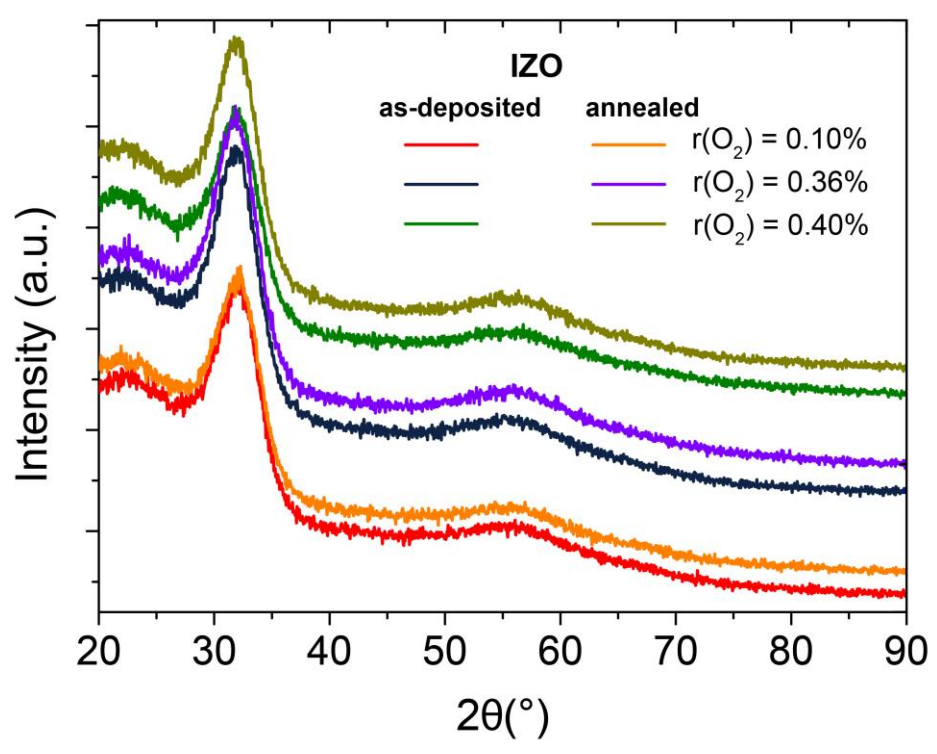


Fig. 1. GI-XRD patterns of a-IZO films on glass substrates with different oxygen partial pressures. Data is offset for clarity.

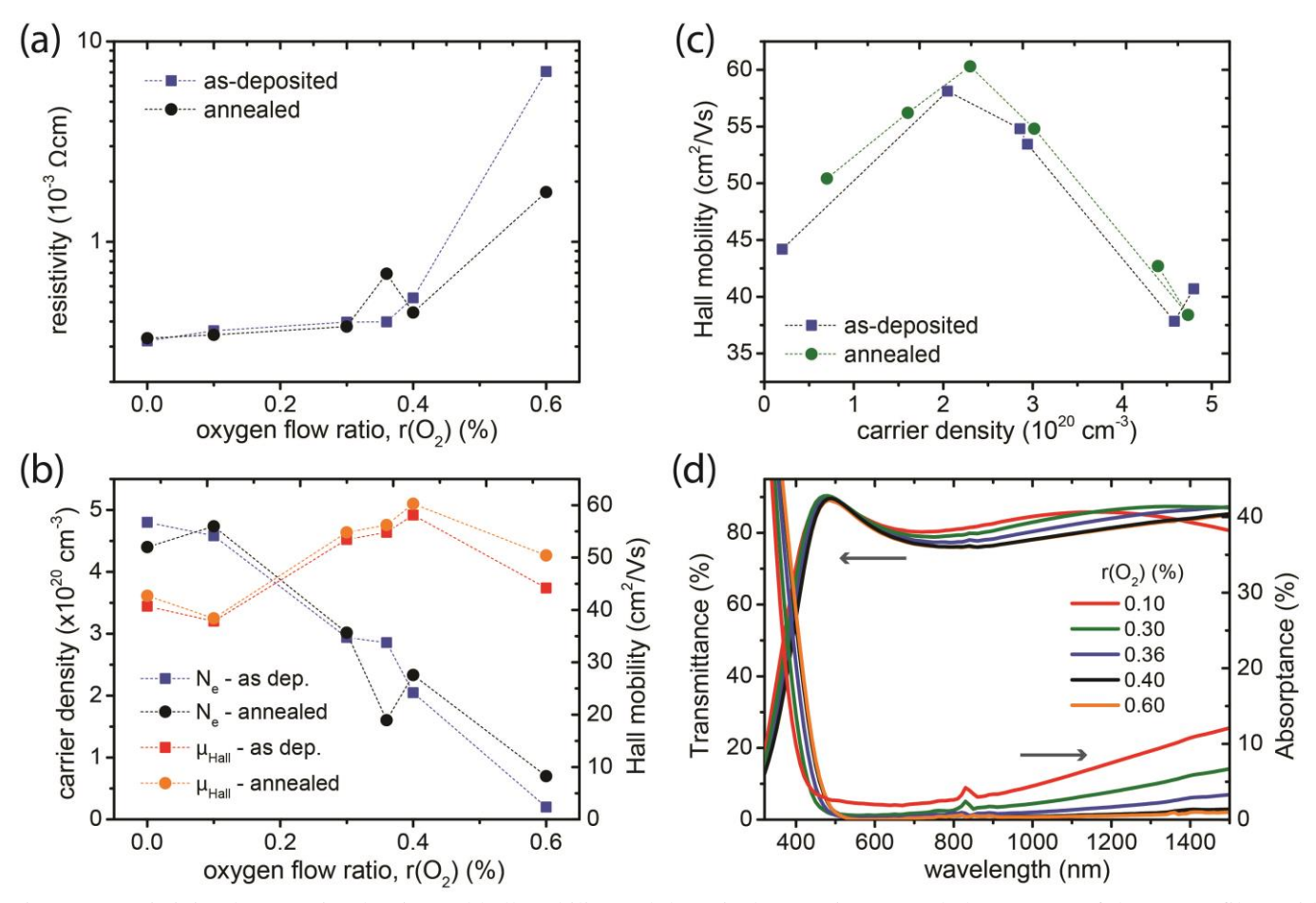


Fig. 2. a) Resistivity, b-c) carrier density and hall mobility and d) optical transmittance and absorptance of the a-IZO films with varying oxygen flow ratios $r(O_2)$ during sputtering deposition.

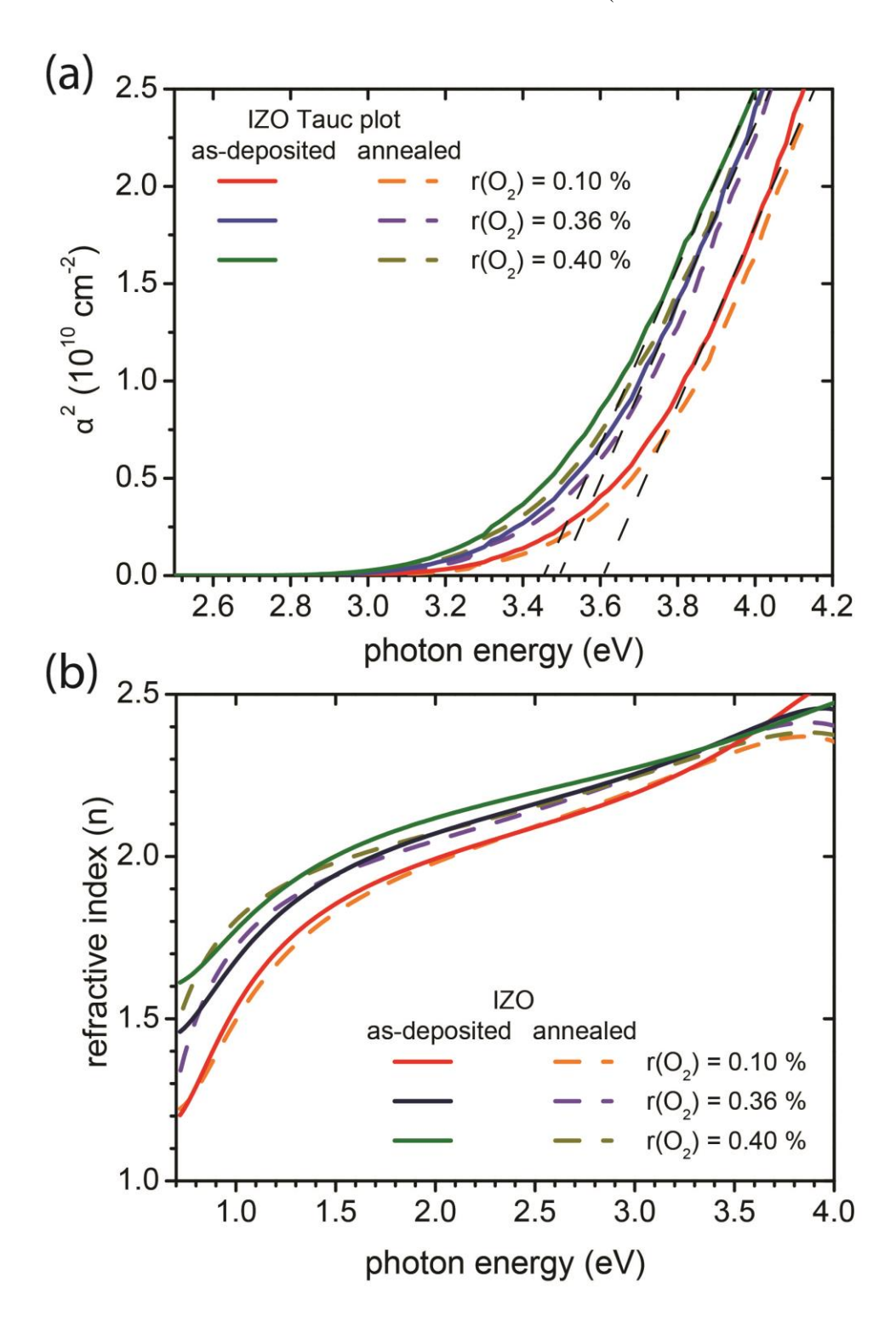


Fig. 3. a) Tauc plot and b) refractive index of the a-IZO thin films with varying oxygen flow ratio r(O₂).

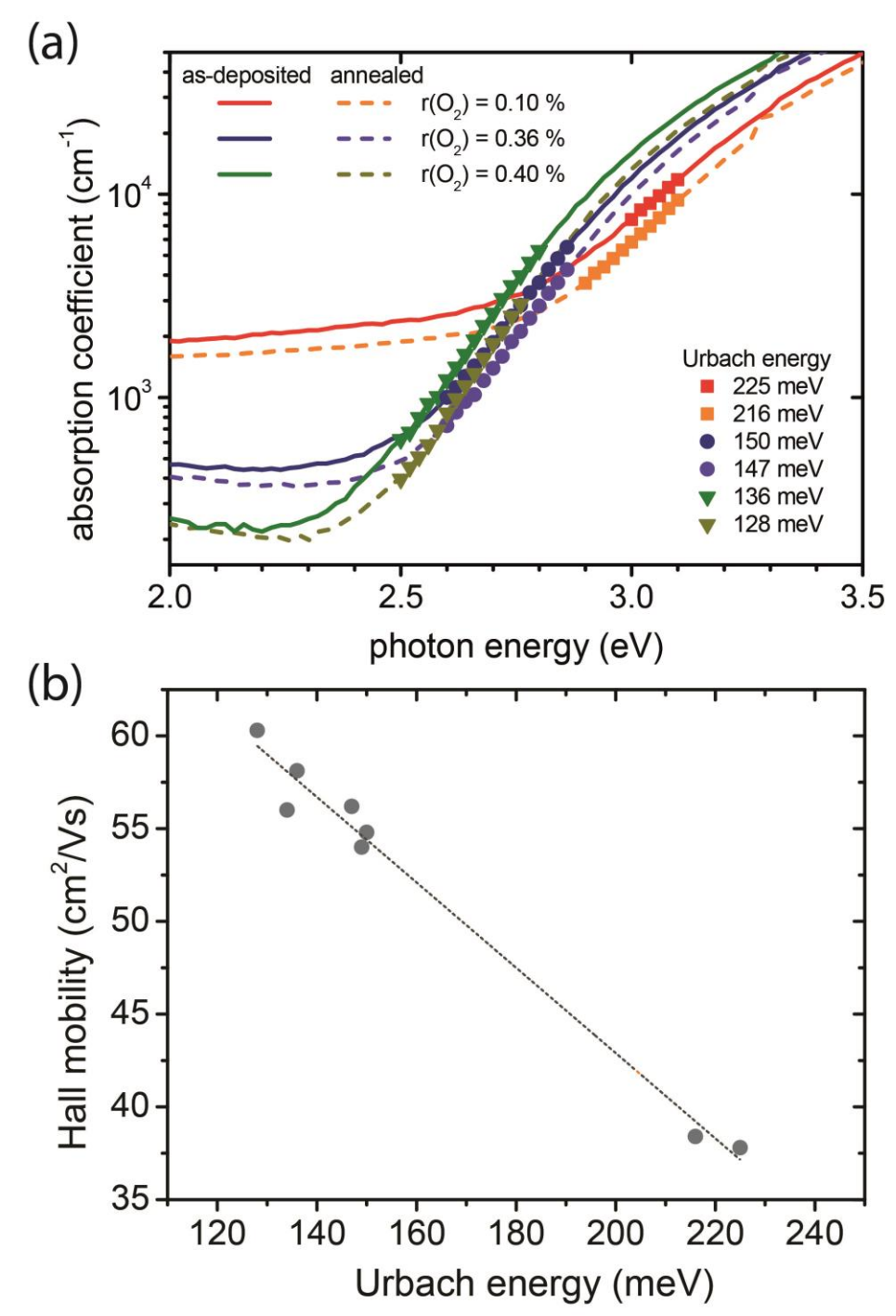


Fig. 4. a) Absorption band edge of a-IZO thin films with varying oxygen flow ratio $r(O_2)$. The round symbols indicate the slope used to extract the Urbach energy values for each sample. b) Relation between the Hall mobility and Urbach energy for the a-IZO layer.

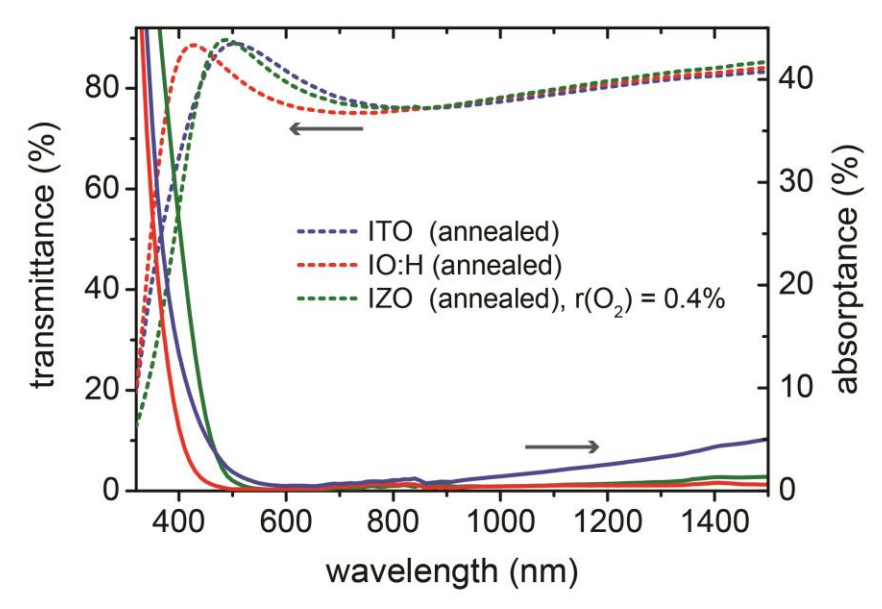


Fig. 5. Optical transmittance and absorptance of ITO, IO:H and a-IZO thin films.

Table 1 Electrical properties of ITO, IO:H and a-IZO thin films.

TCO	N (10 ²⁰ cm ⁻³)	μ (cm²/Vs)	ρ (10 ⁻⁴ Ω cm)	σ (Ω^{-1} cm ⁻¹)	R_{sh} (Ω sq) d = 100 nm
ITO (as-dep)	0.5	47	24	414	240
ITO (annealed)	2.4	25	10	960	100
IO:H (as-dep)	3.8	54	3	3283	30
IO:H (annealed)	1.7	115	3.2	3128	32
IZO, r(O ₂)=0.4% (as-dep)	2.1	58	5.1	1949	51
IZO, r(O ₂)=0.4% (annealed)	2.3	60	4.5	2208	45

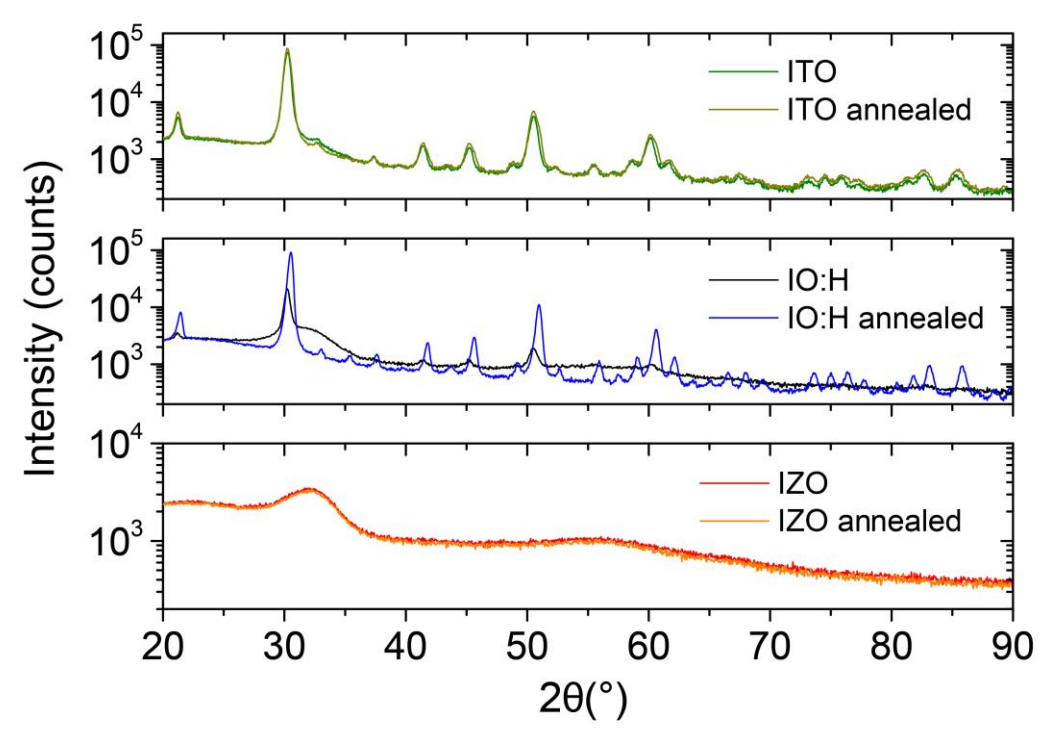


Fig. 6. GI-XRD data of the ITO, IO:H and a-IZO thin films as-deposited and annealed at 190 °C in air for 20 min.

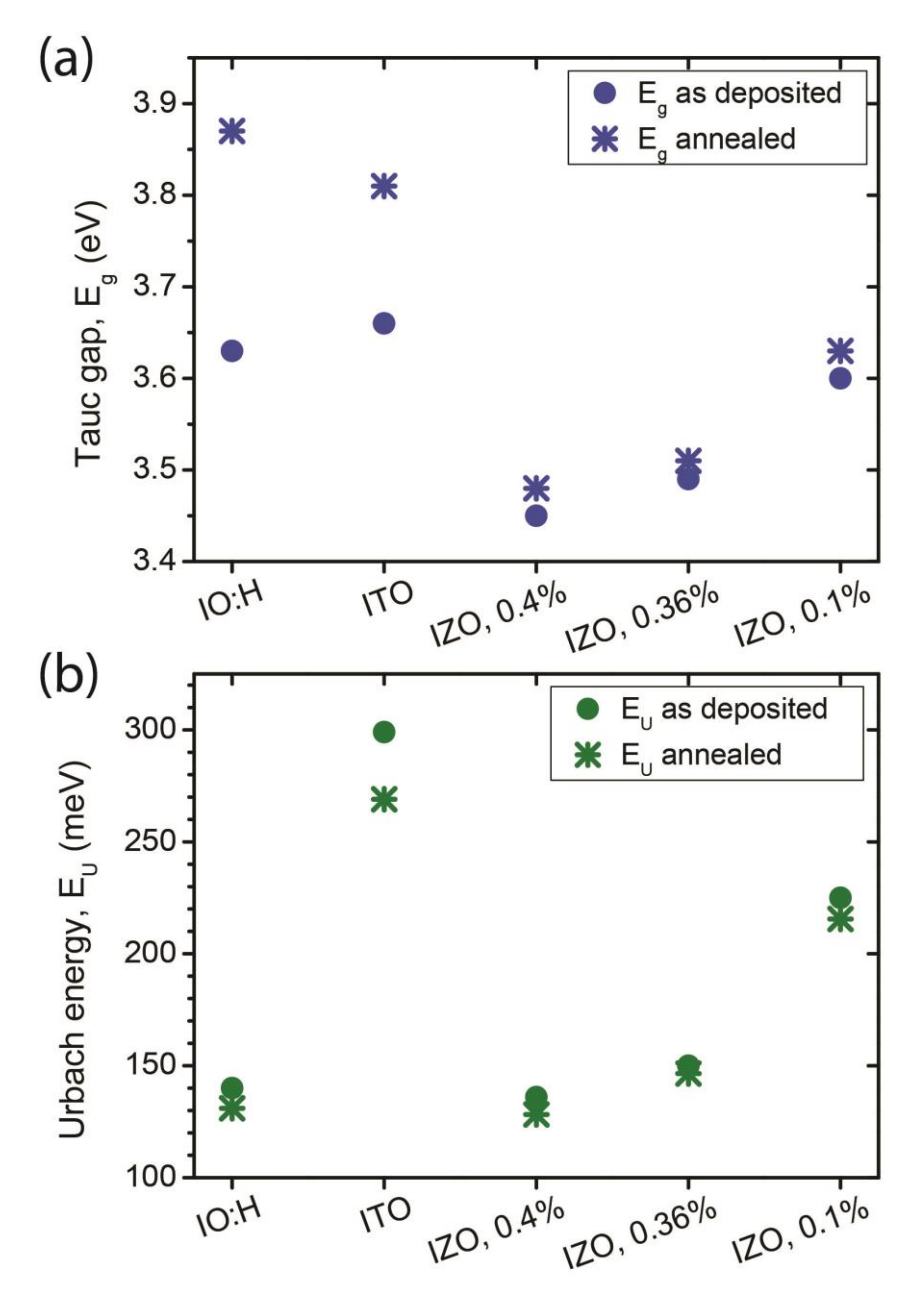


Fig. 7. a) Tauc gap and b) Urbach energy of ITO, IO:H and a-IZO thin films.

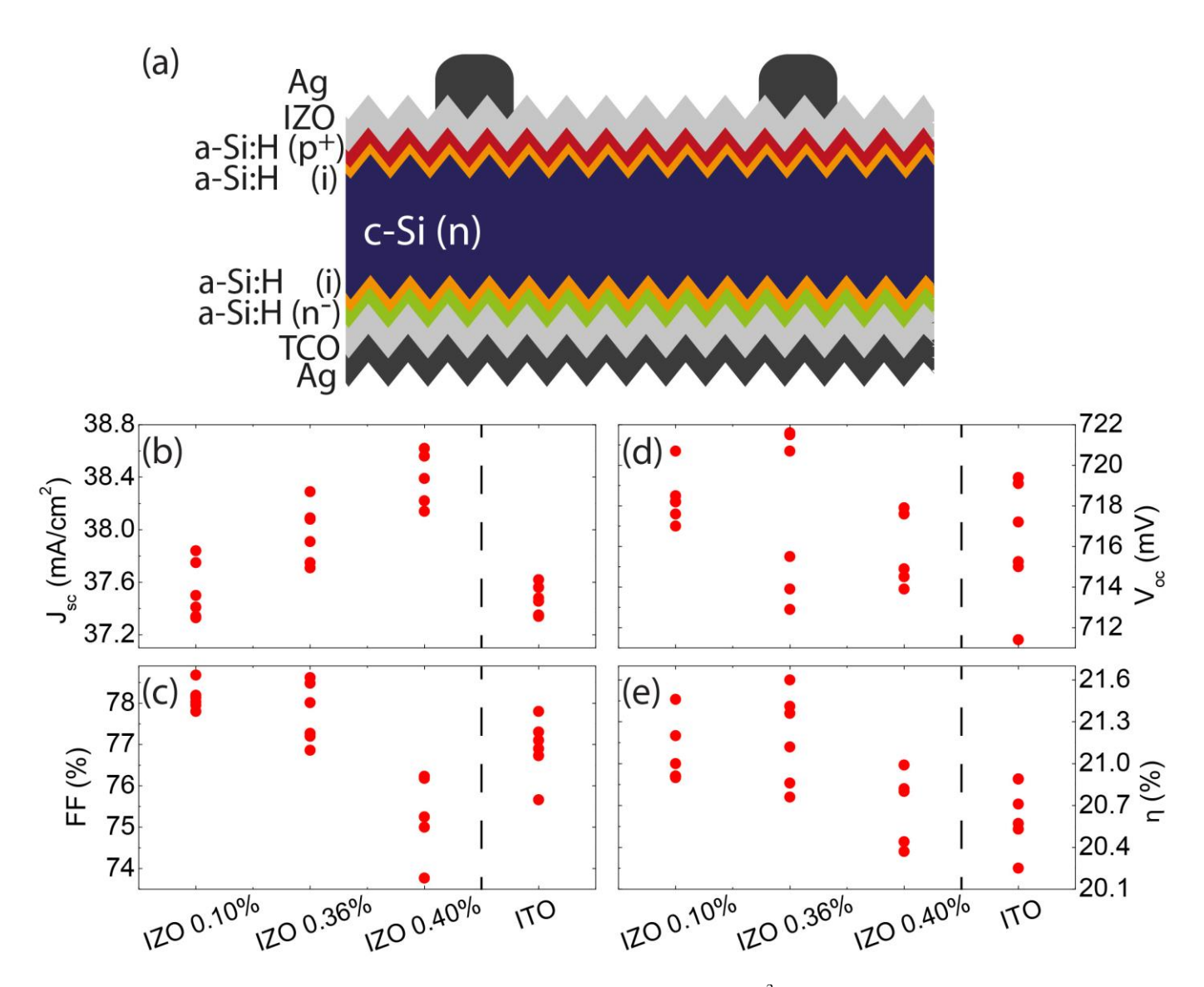


Fig. 8. Output characteristics extracted from current-voltage measurements of 4 cm² solar cells with varying front TCO. (a) Short-circuit current density (J_{sc}), (b) open-circuit voltage (V_{oc}), (c) fill-factor (FF), and (d) conversion efficiency (η).